Experimental study on the thermal comfort in the room equipped with a radiant floor heating system exposed to direct solar radiation

Tianying Li, Abdelatif Merabtine, Mohammed Lachi, Nadia Martaj, Rachid Bennacer

Experimental study on the thermal comfort of the room with a radiant floor heating system while exposed to direct solar radiation

Tianying Li[a,b,], Abdelatif Merabtine[a,b], Mohammed Lachi[a], Nadia Martaj[a,b] and Rachid Bennacer[c]*

[a] *MATIM, Université de Reims Champagne-Ardenne, Reims, 51100, France*

[b] *EPF Campus de Troyes, Troyes, 10000, France*

[c] *LMT/ENS-Paris-Saclay/CNRS/Université Paris Saclay, Gif-sur-Yvette, 91190, France*

Abstract:

In buildings with highly glazed facades, the main drawback of radiant floors is the overheating problem when exposed to direct solar radiation. Combined with local climate data from Troyes, an experimental investigation was performed under various exposure duration 2, 4, and 6 hours with different solar intensity scenarios that were experimentally realized by a heating film. Indoor air temperatures and floor surface temperature were measured. Obtained results showed that the maximum floor surface temperatures all exceeded the limitation of 29°C during the sunshine durations. When the sun patch was applied on the floor, the building type changed from category A to category B in terms of the vertical air temperature difference. To sum up, the sun patch indeed gave rise to floor overheating problems in the case of the existing control system, and the case of 6h sunshine duration with an intensity of 718 W/m² would lead to the worst living conditions taking all factors consideration. The findings and insights of this study will provide an experimental database for designers and engineers.

Keywords:

Floor heating system; Sun patch; Thermal comfort; Overheating; Experiments

* Corresponding author.
E-mail address: tianying.li@etudiant.univ-reims.fr (T. Li).

1. Introduction

Sustainable development has been at the heart of many countries' policy with the energy consumption increasing, which is dedicated to meet the needs of the present without harming the interests of future generations. In Europe, the final energy consumption in 2018 showed three dominant categories: transport (30.5%), households (26.1%) and industry (25.8%), and the main use of energy by households was for space heating (63.6%) [1], which placed the heating usage as one of the primary energy consumers. To meet the energy-saving demand, it's vital to improve the efficiency of the heating system.

Compared with conventional heating methods, the radiant heating system becomes more and more popular due to numerous advantages, including a better thermal comfort, an improved energy efficiency, a better repartition of the heat flux density, and being convenient to be combined with a renewable energy sources [2-4]. Radiant heating systems are mainly divided into three types: embedded surface systems, thermally activated building systems and radiant panel systems [5]. When it comes to embedded systems, known as floor heating systems (FHS), the whole floor surface is used as the heating surface absorbing heat from heating pipes that are usually embedded in the floor. Heat transfer takes place mainly by thermal radiation between the surface of the floor and the surroundings. The indoor air temperature is controlled by regulating the hot water temperature and volume flow rate via a system of valves, pumps and thermostats.

In last decades, a number of numerical and experimental researches was performed to investigate the thermal behaviour of FHS. Merabtine et al. [6] developed and validated a semi-analytical model based on the combination of Design of Experiments method and Finite Difference method, which was of significant practical use for building engineers and designers. Zheng et al. [7] developed a detailed mathematical model solved by Ansys Fluent® for a radiant floor heating system. Four current test standards in China, Europe, America and Japan were simulated with same samples. The relative deviation of heat output of circulated hot water was ranged from 2% to 7% and the non-heating surface temperature was the important factor that affected the heat output and the radiant surface temperature. Cho et al. [8] investigated the thermal performance of the conventional Korea standard radiant floor heating system with polybutylene pipe (PB) and a low-temperature system with capillary tube (CT) in an experimental test and simulation model and found that the thermal comfort from PB model is lower than that of the model with CT.

For further energy-conservation, a floor heating system combined with phase change material has attracted some interests [9,10]. Besides, the low grade energy utilization technology has got development and application as well, mainly containing ground source heat pump [11] and solar heating system [12,13] used in floor heating systems.

Because of the significant impact of the slab's thermal inertia, an floor heating system may not be able to react instantly to a sudden change of thermal loads induced by outdoor climatic conditions or occupants' behaviors. Consequently, this will break the thermal equilibrium between a human body and its surroundings and make occupants thermally uncomfortable. In this case, an appropriate control system is needed. At present, there are about four basic reactive control strategies implemented in actual buildings including ON/OFF control, supply temperature control, pulse width modulation (PWM) and proportional–integral–derivative (PID) control [14-18], which modulate supply temperature or water flow based on indoor or ambient temperatures to achieve the desired set point. The mean radiant temperature [19] may be included to provide the controller feedback as well. As a result, the operative temperature, which is the weighted average of the air and radiant temperature of the surrounding surfaces, should be investigated to contrast with the indoor temperature in terms of system regulation. Athientis [20] conducted a numerical study on the effective room temperature under various control strategies with the constant and the half-sinusoid setpoints. The results indicated that the half-sinusoid setpoint profile had a rapid response capability to outdoor temperature variation, particularly with operative temperature control. Brideau et al. [14] compared different combinations of controllers and floor constructions by simulation for use in a house with high variable solar gains and found PID and outdoor temperature reset with indoor temperature feedback controllers generally perform the best for all cases in the trade-off between the heating energy and occupant comfort.

Furthermore, in addition to the above control strategies, it is interesting to combine it to a predictive control that mainly remains nowadays at theory stage because of its complexity. Candanedo et al. [21] facilitated the application of predictive control techniques in homes with large solar gains and significant thermal mass through a simple transfer function model. Hu et al. [4] developed a model predictive control for FHS with Trnsys®-Matlab® co-simulation, which could simultaneously consider all the influential variables including weather conditions, occupancy and dynamic electricity prices to implement automatic and optimal preheating.

Nevertheless, when it comes to the floor heating systems exposed to the direct sun radiation, few experimental studies have been carried out to address the overheating concerns due to the sun patch. Olesen [22] used electrical heated blankets placed on the floor to simulate solar, occupant and lighting gains, with a peak value of 15W/m² of total floor area, in order to compare the ability of controlling of three different heating systems. Beji et al. [23] carried out an experimental work on the impact of direct sun radiation on the thermal reponse of FHS. They observed an overheating due to the direct solar radiation simulated by a heating film, which was set to 700 W/m² representing the solar intensity on a clear sky day in the winter season. This study placed emphasis on the comparison among various sun patch (the heating film) locations with regard to the incoming

direction of the solar radiation. Benzaama et al. [24] developed a combined model using Trnsys® and Fluent® to simulate the effect of the sun patch on a heating floor under transient climatic conditions of Algeria. The maximum floor surface temperature difference reached 14 °C between the solar irradiated zone and the shaded zone, which had a great influence on thermal comfort. Rodler et al. [25,26] developed a 3D refined transient thermal model of energy efficient room envelope to study the impact of a time-varying sun patch projected from a single window. This work concluded that the location of the sun patch had a strong influence on the surface temperature distributions. They clearly showed the influence of the sun patch on the temperature distribution of the ground surface at 16:09 for the 11th may 2013, which ranged between 23 to 32°C. The developed numerical model was validated by measurements carried out in a thermal test cell without a floor heating system. Based on this study, Almeida Rocha et al. [27] confirmed that pixel counting technique implemented in Domus® software could improve the accuracy and speed of calculations for sun patch on the internal surfaces, especially for buildings with complex geometries (non-convex zone) compared with the Energy Plus®.

To sum up, for our knowledge, most of the researches mentioned above only focus on the simulations or the observed sun patch in a test cell no-equipped with a FHS. The existing limited experimental study didn't involve the impact of sunshine duration in real use and consider the local thermal comfort. Hence, the purpose of the present study is to experimentally simulate the sun patch by a heating film, placed on a real FHS, under different exposure periods in order to fill the research gap by: (i) Quantifying the overheating due to sun patch for different exposure periods on a real FHS controlled by a PID regulation. (ii) Estimating the local thermal comfort according to ASHRAE [28,29] and ISO7730: 2005(E) [30] standards. (iii) Opening-up perspectives to develop new control strategies that take into account solar radiation effect for a better living space.

2. Material and methods

2.1. Experimental set-up

The experiments were performed at EPF engineering school in Troyes, France. A full-scale test cell with available space of 11 m² of area and 2.1 m of height was used in this study. The test cell is composed of two adjacent well-insulated rooms which are constructed by wood and insulated hemp wool and wood fibres, as shown in Fig. 1(a). To experimentally simulate the direct sun radiation on the floor, a heating film (Fig. 1(b)) with a dimension of 0.400 m×1.065 m was applied on the surface of the radiant slab. Its electric power is adjustable from 315 W/m² to 718 W/m². The heated room is equipped with a floor heating system including a 51 m long of crosslinked polyethylene tube embedded in the bottom of a 5 cm thick of anhydrite screed slab and the top of a 6 cm thick of insulation layer. The inner and outer diameters of the tube are 13mm and 16mm, respectively. Fig.

1(c) shows the schematic diagram of cross section view of the radiant slab. In the test cell, no mechanical ventilation system was utilized. The volume flow rate of supply water is controlled by means of a thermostatic valve to keep the indoor air temperature within the set point and the inlet water temperature is set to 32°C. The cold room will provide the cold climate to simulate the outdoor sunny cold day in winter season via a air conditioner. The rooms are separated by a highly insulated wall with a small opening to simulate natural ventilation. More details about the structure of this test cell were shown in reference [6]. Properties of materials mentioned above are given in Table 1.

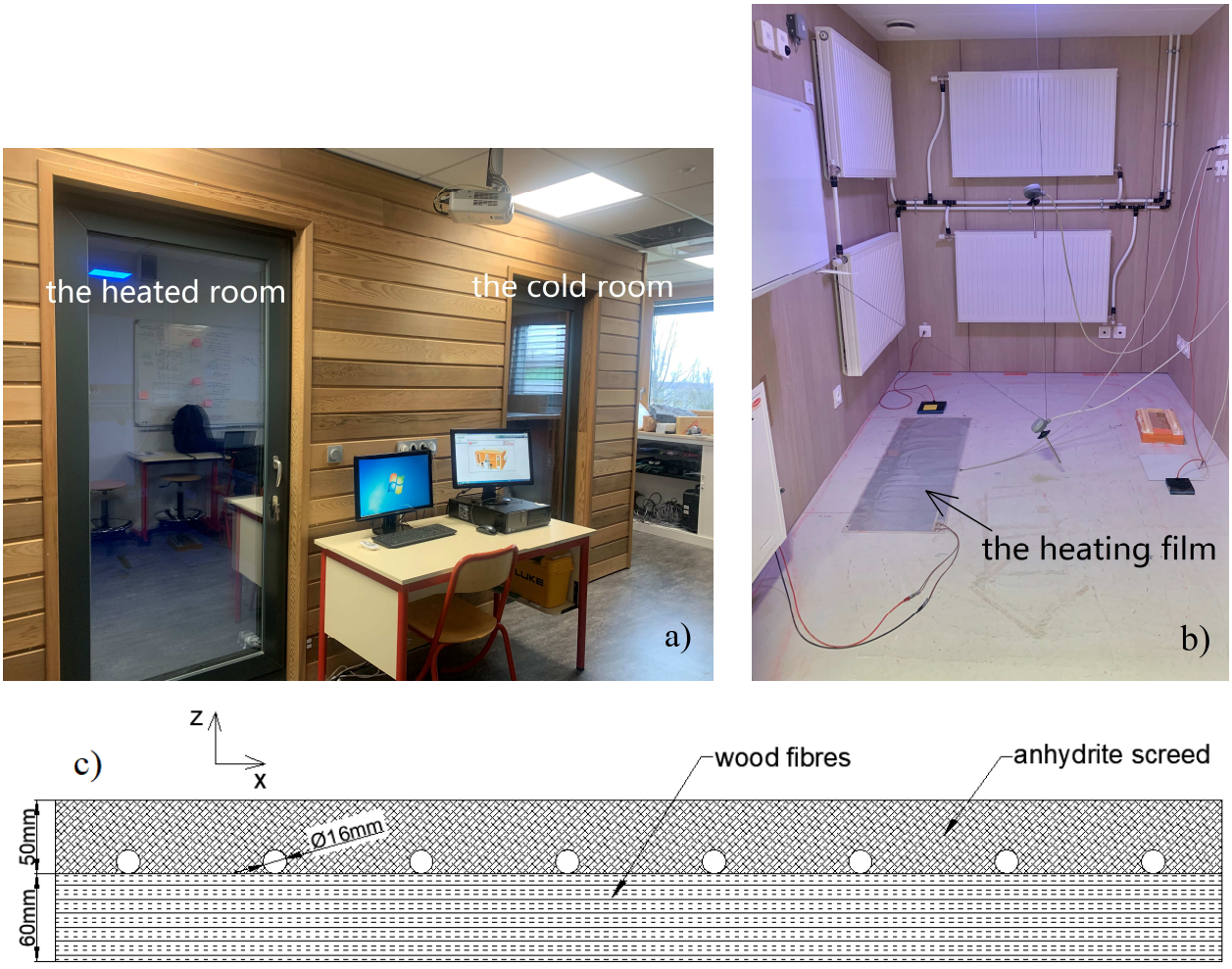

Fig. 1. (a) Full-scale test cell. (b) Interior view of the heated room. (c) Schematic diagram of cross section view of the radiant slab.

Table 1
Material properties.

	Hemp wool	Wood fibres	crosslinked polyethylene	anhydrite screed
Density *kg/m³*	25	40	920	1900
Thermal conductivity *W/m•K*	0.04	0.04	0.4	1.2
Specific heat *J/kg•K*	1300	2100	2300	1000

2.2. Experimental method

For clear sunny days in winter, it was assumed that a maximum of 700 W/m² solar radiation was transmitted through the test room window based on measurements [14]. Fig. 2 shows the collected daily data containing the sunshine duration, maximum direct solar radiation and outdoor average temperature in February 2018 from the weather station located in Troyes [31]. It's worth noting that the solar intensity has reached or even exceeded 700 W/m² while presenting colder outdoor temperature for the highlighted days, which is visibly adverse to room comfort under PID control who regulates the supply temperature against the outside temperature. It's possible to get overheated in the cases of high supply temperature and strong solar radiation. Taken together for the whole month, the outdoor average temperature basically rises and falls around 5°C, and the sunshine duration is mainly concentrated in 2, 4 and 6 hours. The actual data will serve as a reference for testing conditions. Fig. 3 shows the different solar radiation intensity values appearing at every time point from 10am to 4pm in February based on the collected weather data from the weather station [31]. One can find that even at 10am, the solar intensity also reached 700 W/m² on a certain day. To close to the true circumstance and observe the worst overheating effect, we selected the same maximum power intensity provided by the heating film, i.e. 718 W/m², which was equivalent to 55.6 W/m² of total floor area. Fig. 4 illustrates the applied heat flux density of the sun patch imposed on the floor. The exposure duration Δt was a key factor that was varied from 2 to 6 hours, meanwhile the heat flux density keeping constant. The cold room was fixed at 5°C as the outdoor condition of the heated room.

The monitored test cell is illustrated in Fig. 5 and it shows the sensors' locations. The heating film (point 6) was kept in the same position in order to only simulate a certain building orientation. The measuring points 1, 2 and 3 were selected to measure indoor air temperature according to Z direction. The temperature measured at point 1 (Z = 1.78 m of height) was the reference

temperature. The system would control the opening rate of thermostatic valve depending on the temperature difference between the reference temperature and the setpoint. The heights of points 2 and 3 on the central axis of the structure from the floor were 1.1 m and 0.1 m respectively to estimate the temperature gradient between head level and ankle level for a seated person according to ISO standard [30]. The floor surface temperature was monitored by a temperature sensor at point 4 located at 5 cm from the heating film according to Y direction. Also, heat flux densities of sun patch toward floor, and floor toward air were measured by two heat flux meters located at points 5 and 7, respectively. In addition, the inlet and outlet water temperatures (numbered points 8 and 9) were measured, and a water flow rate meter was installed on the inlet water tube. All the aforementioned measuring points and measuring equipments characteristics are given in Table 2.

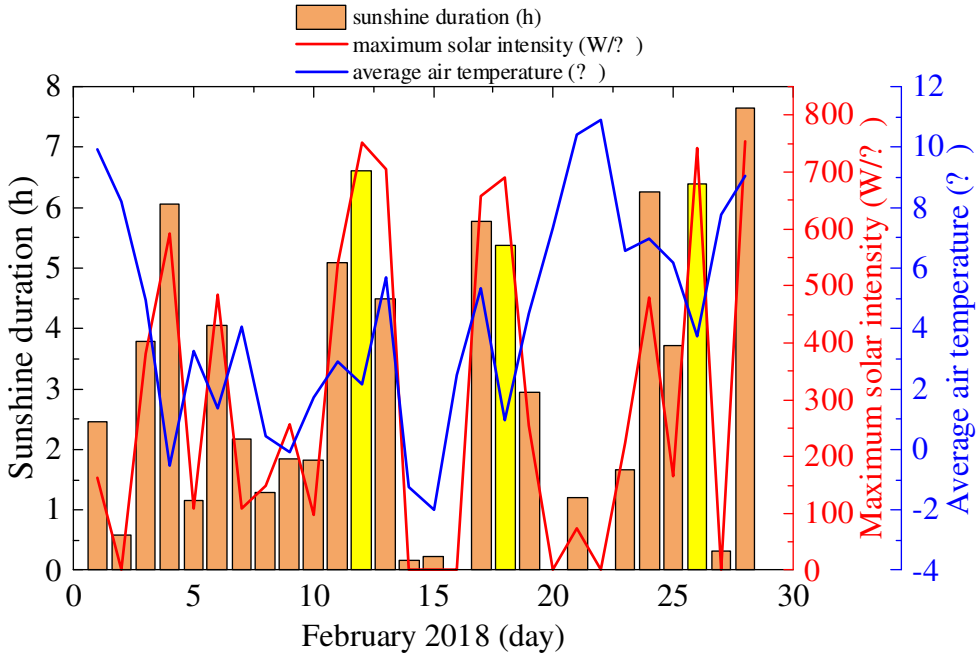

Fig. 2. Collected weather data of Troyes in February 2018.

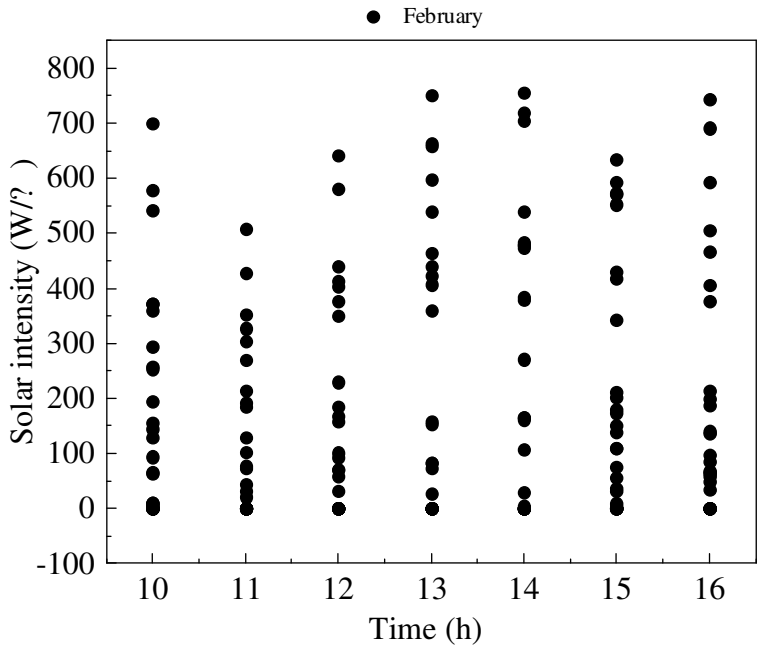

Fig. 3. Different solar radiation intensity values appearing at every time point from 10am to 4pm in all days of February.

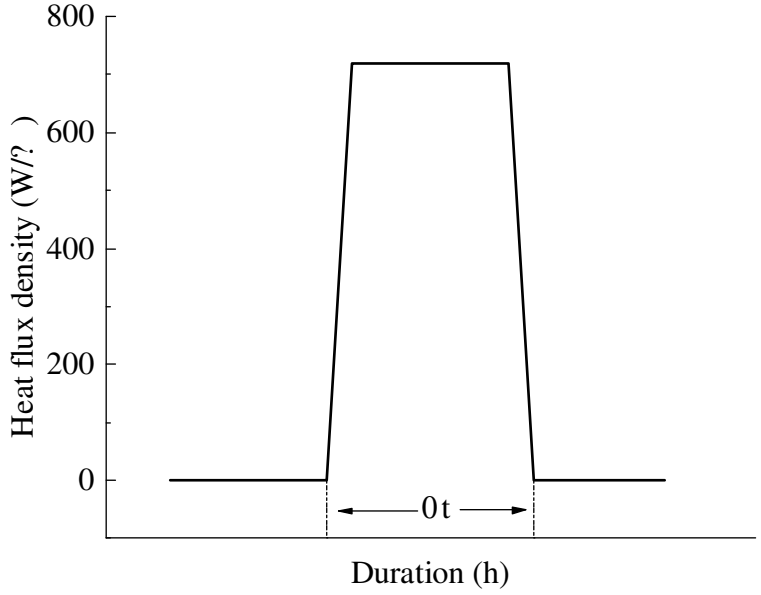

Fig. 4. Heat flux density of the sun patch.

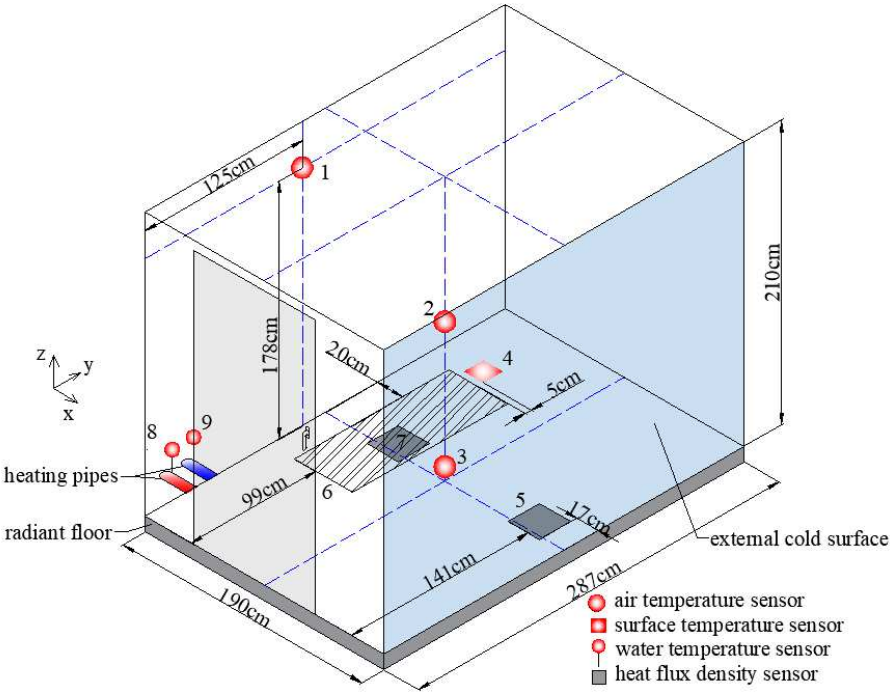

Fig. 5. Arrangement of measuring points.

Table 2
Measuring instruments.

Instrument	Number	Measuring points	Measuring range	Accuracy
Temperature sensor (KLH 100)	1	1	[-50, 50]°C	±0.5°C at 25°C
Surface temperature sensor (TEPK PT1000)	2	8, 9	[-20, 80]°C	±0.3°C at 0°C
Temperature sensor (PT 1000)	3	2, 3, 4	[-20, 100]°C	±0.3°C at 0°C
Flux meter (AHLBORN FQA019C)	2	5, 7	[-260, 260] mV, <120°C	±0.01 mV, ±0.12°C

In this experimental study, the air set point temperature was set to 21°C. In the first scenario, the floor heating system was turned on to heat the radiant slab until the indoor air temperature reached the set point value and got the steady state. The aim of this scenario was to analyse, as a benchmark, the thermal response of the FHS without applying a sun patch. In the second and the third scenarios, when the indoor air temperature was kept within the set point, the heating film was turned on for different heating duration of 2, 4 and 6 hours to investigate the influence of the sun patch on the FHS and indoor thermal comfort. Finally, the indoor thermal comfort would be evaluated according to ASHRAE [28,29] and ISO7730: 2005(E) [30] standards.

3. Results and discussion

3.1. First scenario: Benchmark experiment

Fig. 6 shows the transient temperature measurements and thermostatic valve opening rate. At the beginning, the thermostatic valve was fully opened so as to heat the chamber quickly. Then, it began to close as soon as the referenced air temperature got close to the set point. Due to the thermal inertia of the heating slab and the time-taking shutdown process of the thermostatic valve, the referenced air temperature and the floor surface temperature would continue to rise and eventually reached 23.0°C and 29.1°C, respectively. After that, the thermostatic valve kept off until the referenced air temperature decreased to reach the setpoint temperature of 21°C. In the steady state, the indoor environment remained stable between opening and closing of the valve, since the air temperature fluctuated around 21 ± 0.5°C. It could be concluded that the thermostatic valve regulates well the air temperature according to the set point by controlling the water volume flow rate.

As a reference temperature, the sensor was fixed on the left wall at 1.78 m height from the floor instead of in the central axis compared to the other two air temperature sensors. We found the difference among air temperatures that the 1.78 m height was lower than the 1.1 m height, and higher than the 0.1 m height at the steady state. Such variation was the consequence of the internal natural convective flow. In the heated room, the heated air usually ascends from the center and descends along the walls to be the cooled air. Besides, under this coordinate scale, the transient air temperatures had nearly synchronous cycle fluctuation with the floor surface temperature, and since the sensor location was near the floor, the air temperature at 0.1 m height even kept the same changing trends (with a delay) with the floor surface temperature.

Besides, there was a time delay between the hot water supply and floor thermal response in the heating process as shown in Fig. 7. Fig. 7 describes more detailed control process including the evolution of inlet temperature, floor surface temperature, referenced air temperature and the opening rate of the valve. There are two partial enlarged drawings at the bottom, which show the time delays marked by plaid rectangular regions in the transient and the steady stages, respectively. The valve was fully opened while starting the floor heating system, then the inlet hot water came later, and the thermal response of the floor surface took about 6 minutes. At the steady stage, the maximum opening rate of the valve was about 10%, and the time delay between the hot water supply and floor thermal response ranged from 15 to 40 minutes. Apart from the inherent thermal inertial of the slab, obviously, the time delay depends on the mass flow rate, and the smaller mass flow rate is, the longer the time delay would be. Actually, the PID control in this study have taken into account it and has some anticipate capacity referring to the valve regulation on the dash-dotted line in the two partial enlarged drawings, which usually takes action before the air temperature

reaches the setpoint. In summary, the present system could meet the general heating requirement via monitoring the air temperature compared with the setpoint.

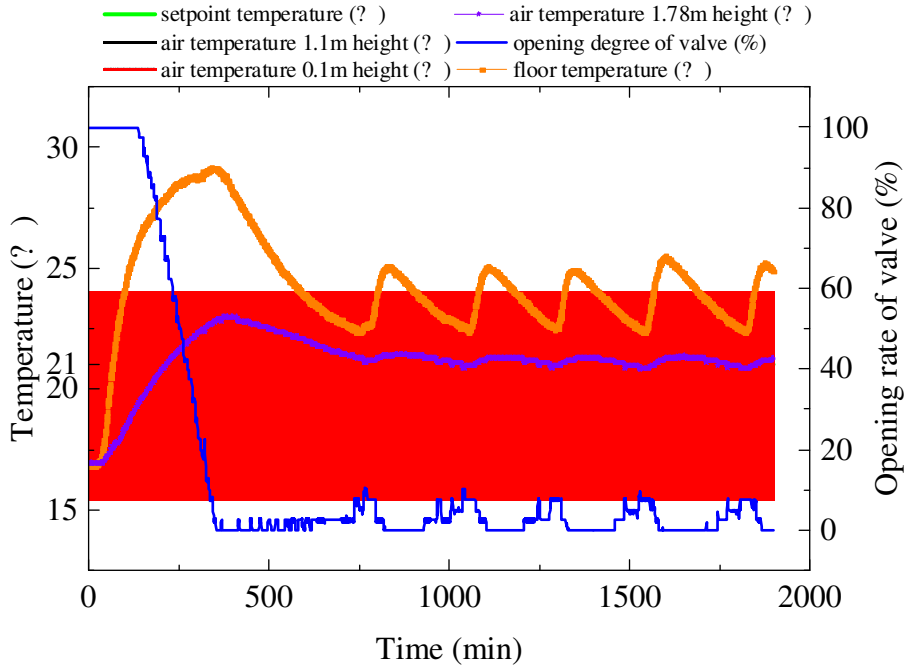

Fig. 6. Measured temperatures and thermostatic valve opening rate for the first scenario.

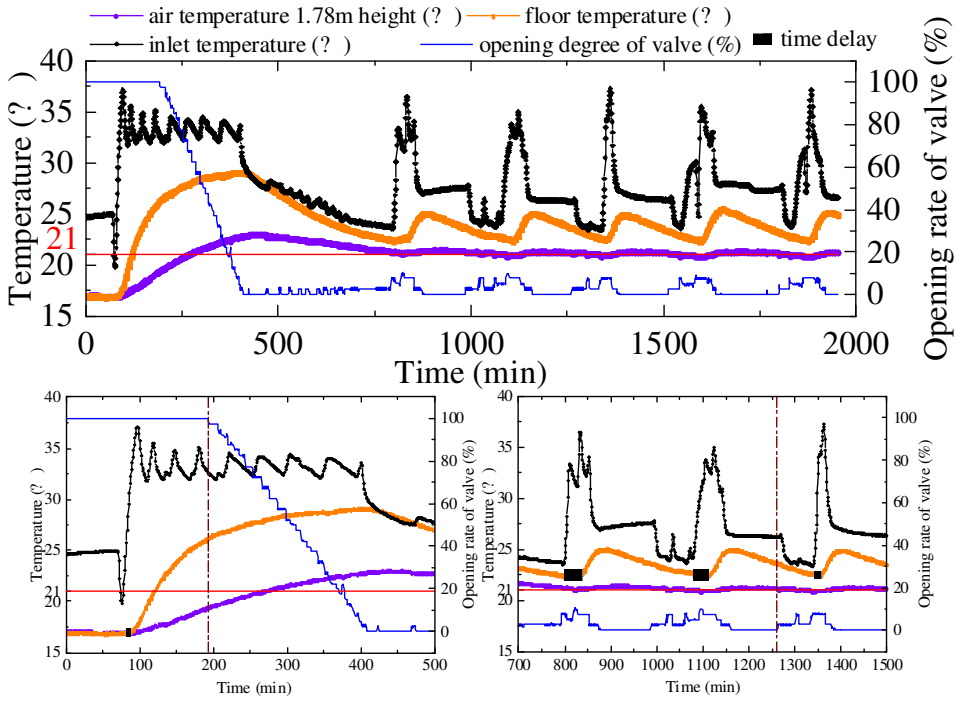

Fig. 7. The detailed control process with two partial enlarged drawings at the bottom.

3.2. Second scenario: FHS with sun patch having constant intensity

In this second scenario, the overheating was estimated when the sun patch was applied on the FHS. Fig. 8 shows the influence of the sun patch during different heating periods, i.e. 2, 4 and 6 hours. Power expended by the heating film converted into heat, of which a very small part was for its own heating because of the light weight with the thickness less than 1mm. Some were absorbed by the floor via heat conduction, and another part were transferred to the indoor air and surroundings by convection and radiation. One could expect that with the floor surface temperature increasing, the temperature difference between the film and the floor was dropping accordingly. As a result we could see that the heat flux density of sun patch toward the floor was decreasing gradually.

ASHRAE [28] recommends a maximum floor surface temperatures of 29℃ in occupied-spaces for comfort reasons in terms of overheating. The air temperature could range from between approximately 19.4 to 27.8℃ [29]. According to the measured data, the maximum air temperature appearing at 1.1m height respectively were 23.9℃, 25.7℃, and 26℃ for 2, 4 and 6 hours of sun patch exposure period and the maximum floor surface temperatures were 29.5℃, 35.7℃ and 37.3℃, respectively. Although the air temperature stayed within the comfort level, this experimental result confirmed the overheating impact on the floor from sun patch and the longer the period exposed to radiation was, the greater the effect was.

The evolutions of the floor and air temperatures were similar with the first scenario before and after the forced sun patch. During the sunshine duration, the sun patch became the main factor instead of the floor to affect the air temperature. As a result, it could be found that the air temperature was no longer synchronous with the floor surface temperature, but with the sun patch. The sensor 4 measuring the floor surface temperature in Fig. 5 located at 5cm distance from the heating film, therefore, there was a time delay involved in this heat transfer process.

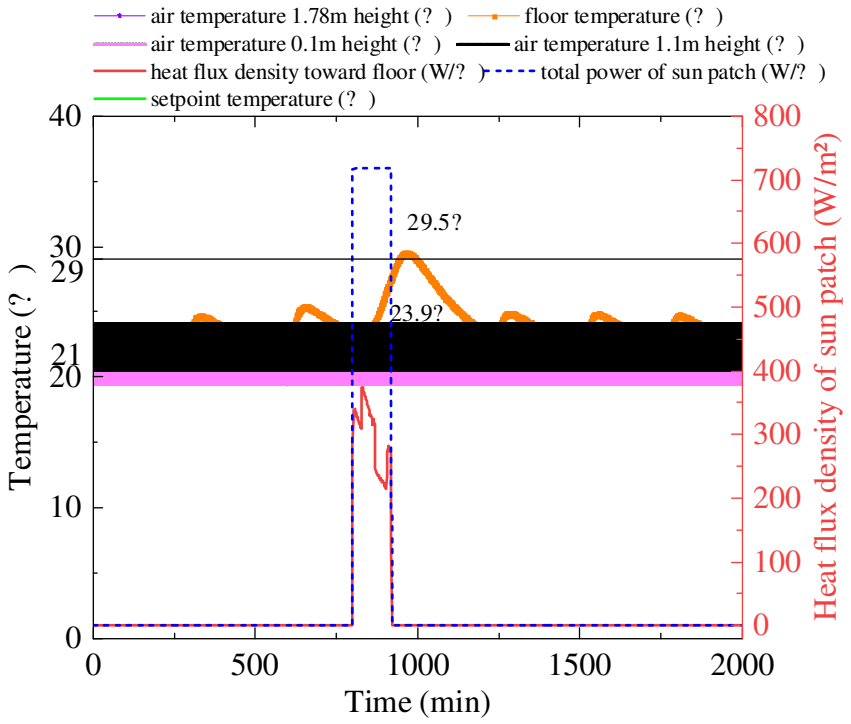
air temperature 1.78m height (?)
floor temperature (?)
air temperature 0.1m height (?)
air temperature 1.1m height (?)
heat flux density toward floor (W/?)
total power of sun patch (W/?)
setpoint temperature (?)
29.5?
23.9?
Temperature (?)
Heat flux density of sun patch (W/m²)
Time (min)
0
500
1000
1500
2000
0
10
20
21
29
30
40
0
100
200
300
400
500
600
700
800

(a) 2h

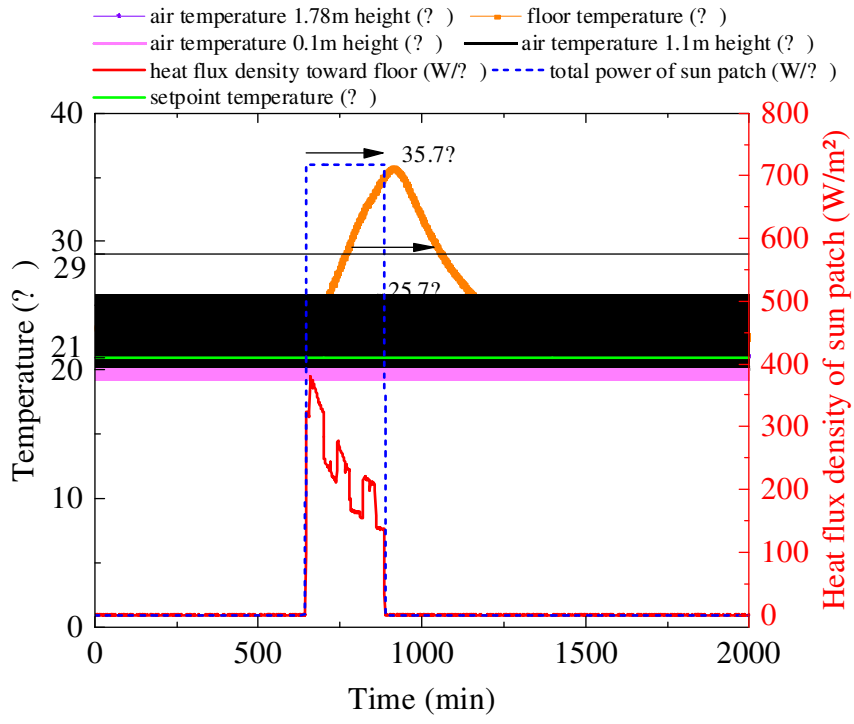
air temperature 1.78m height (?)
floor temperature (?)
air temperature 0.1m height (?)
air temperature 1.1m height (?)
heat flux density toward floor (W/?)
total power of sun patch (W/?)
setpoint temperature (?)
35.7?
25.7?
Temperature (?)
Heat flux density of sun patch (W/m²)
Time (min)
0
500
1000
1500
2000
0
10
20
21
29
30
40
0
100
200
300
400
500
600
700
800

(b) 4h

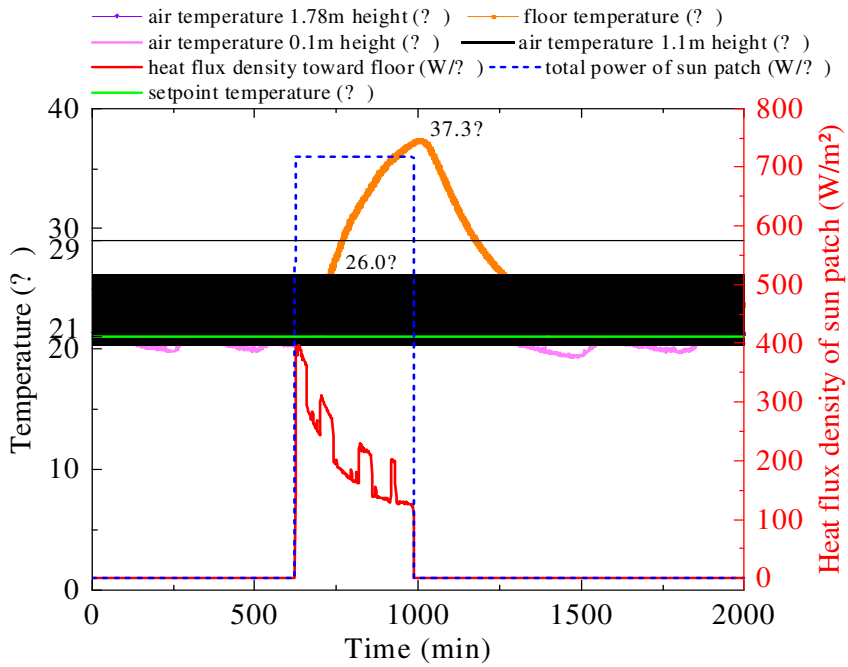

(c) 6h

Fig. 8. The impact of the sun patch exposure duration on the overheating.

Fig. 9 shows the regulation process in the case of 6h of the sun patch exposure period. The thermostatic valve was closed since the indoor air temperature exceeded the set point during the sunshine duration. There was no water supply while the valve was closed. In the meantime, the floor temperature grew rapidly without any system control, and was only affected by the sun patch completely. Although the PID regulation of the floor heating system worked correctly, it couldn't anticipate the thermal input from the sun patch and also couldn't sense the floor temperature through the air temperature control based on the constant setpoint. Based on it, there are some control strategies' improvements in the future. For example, reducing the setpoint value within comfort range or giving a setpoint curve versus the climate data if possible, or monitoring the floor surface temperature with the constant setpoint. In Fig. 9, the outlet temperature ranged from 26℃ to 29℃ at the steady state in the case of 6h of the sun patch exposure period. Therefore, as an available solution, the outlet water probably can be used as the inlet water to cool down the floor while the sun patch is coming and the floor surface temperature is beyond acceptable tolerances.

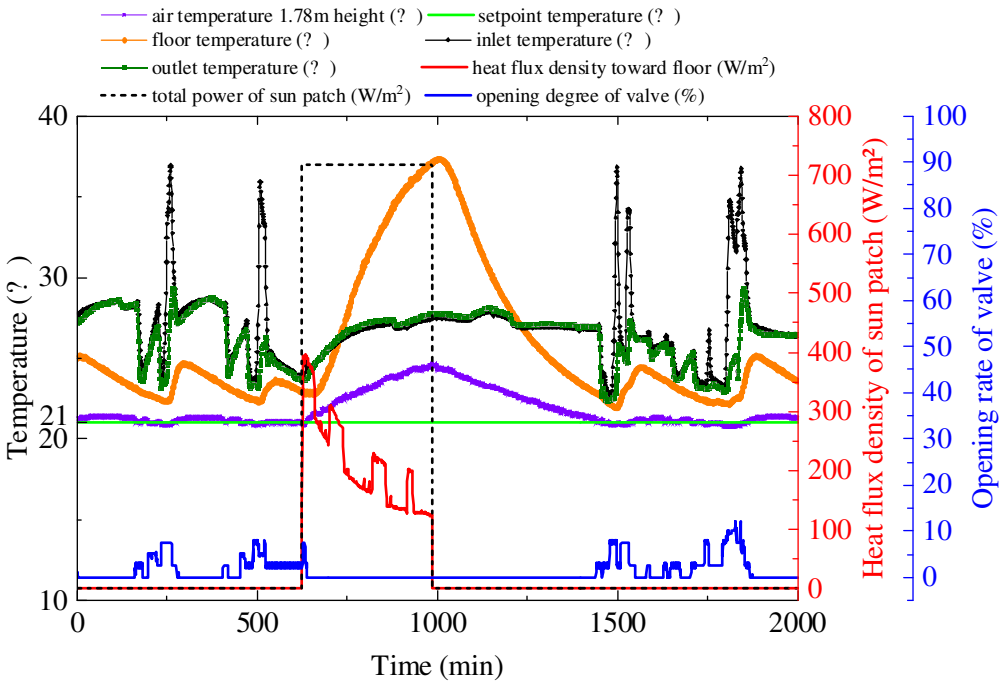

Fig. 9. The regulatory mechanism at heated duration of 6h.

3.3. Third scenario: FHS with sun patch having varied intensity

In the second scenario, we applied the maximum solar radiation intensity as test condition during the sunshine duration of 6 hours in order to investigate the worst-case possibilities. Nevertheless, the solar intensity usually can vary from sunrise to sunset. In fact, the other two experimental tests were performed with the profiles shown in Fig. 10. Profile 1 experimentally represented a sun patch with an intensity of 406 W/m², which was equivalent to 31.4W/m² of total floor area, at the beginning for three hours and 718 W/m² for the remaining three hours. Whereas, profile 2 represented 718 W/m² of solar intensity for the first three hours and 406 W/m² for the subsequent three hours. The other conditions were kept same with those presented above. The results were shown in the Fig. 11.

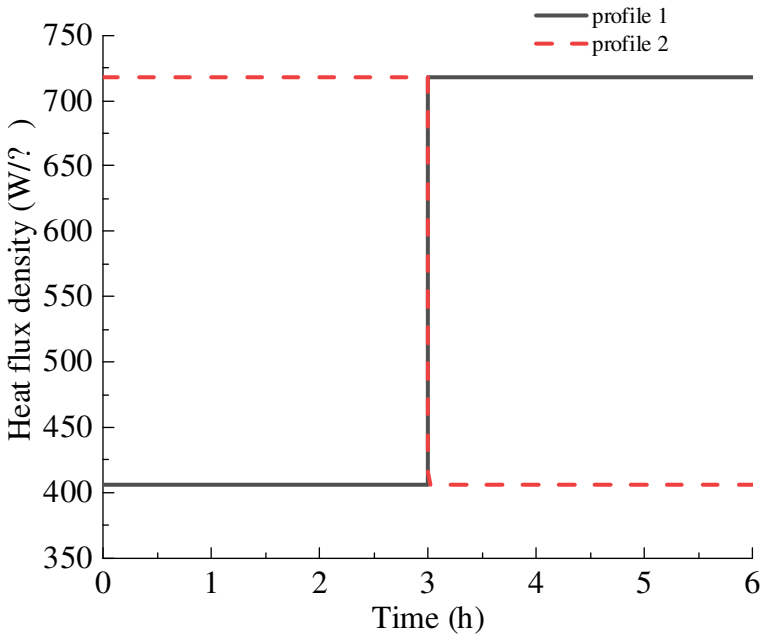

Fig. 10. The intensity change of profile 1 and profile 2.

The maximum floor temperatures for profile 1 and profile 2 reached 36.4℃ and 35.0℃, respectively. These upper limits were lower than those presented in the case of 6h sun patch exposure period (Fig. 8(c)), and it was obvious that the overheating still existed on the floor in the two cases. Correspondingly, the peak values of air temperatures were 25.9℃ and 25.7℃, respectively, staying in the range of the thermal comfort purposes. As previously mentioned, the heat flux through the floor dropt off when the floor temperature increased. Thus, even if the electric power was kept constant, the heat flux density through the floor could be different with change of the floor surface temperature as shown in Fig. 11.

Concerning profile 2, the heat flux density toward the floor had been below 100W/m² in the last three hours in contrast to the one with the least value of 158W/m² in the first three hours for profile 1, although the provided electric power was same with the value of 406 W/m². During those three hours using electric power of 718 W/m², the heat flux density toward the floor presented similar variations, but unlike profile 2, the heat flux density corresponding to profile 1 had a more even distribution because the floor was exposed firstly to softer solar radiation.

In Fig. 11(b), during the last three hours the air temperatures were little changed, and the floor temperature was falling slowly, which meant that the heat energy from the sun patch was too small to maintain thermal equilibrium, so the floor surface temperature reached the maximum value of 35.0℃ just after the first three hours with a time delay, as already explained in the second scenario. Consequently, the maximum floor surface temperature in profile 2 was lower than the one presented in the case of 4h (Fig. 8(b)). In this scenario, the regulation process of the floor heating system was described in Fig. 12. When the sun patch appeared, the air temperature became higher than the

setpoint level and the system closed the valve during the sunshine duration. Beyond that, there was no other adjustment measures from the system to improve the overheating problem under the present regulation mechanism.

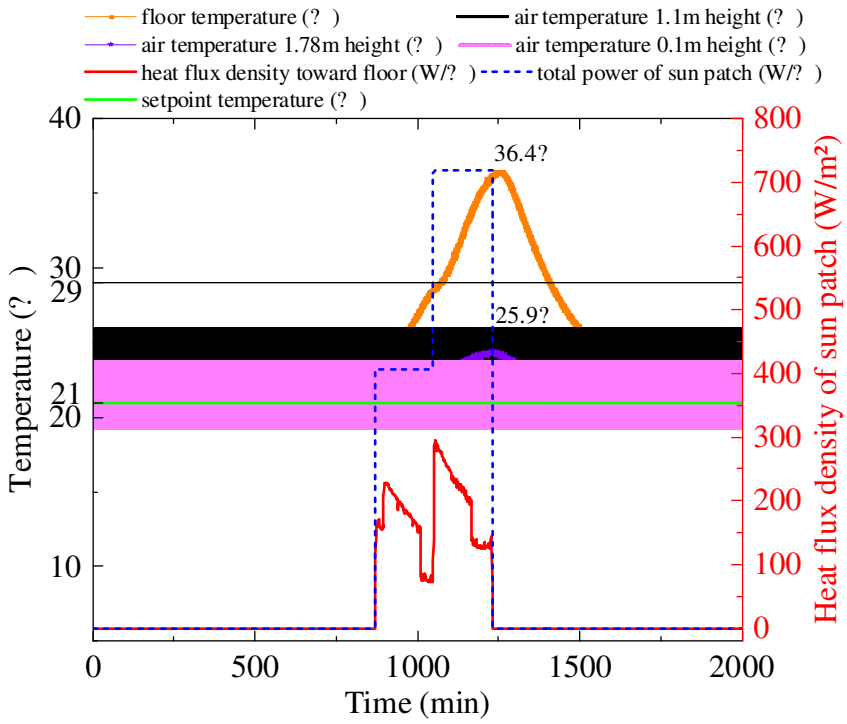

(a) profile 1

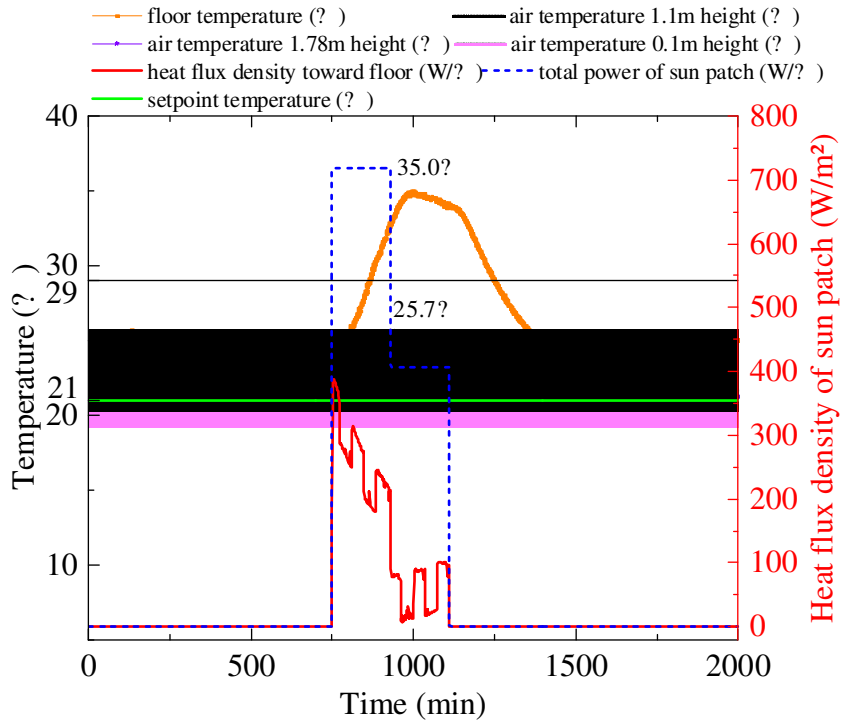

(b) profile 2

Fig. 11. Impact of the sun patch intensity variation on the thermal response of the FHS.

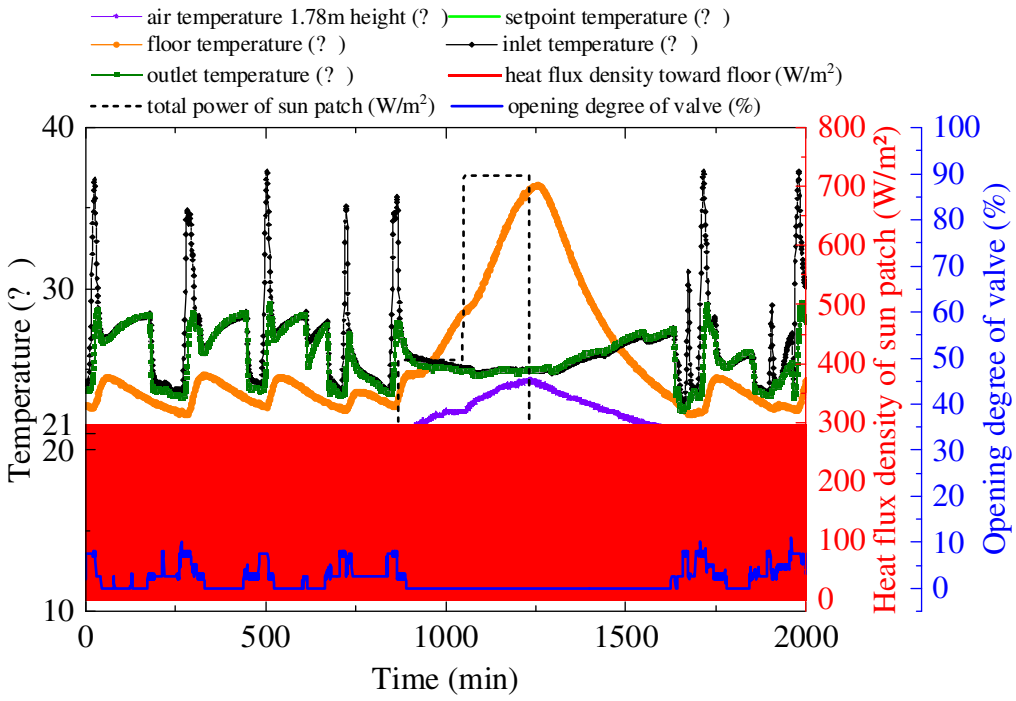

(a) profile 1

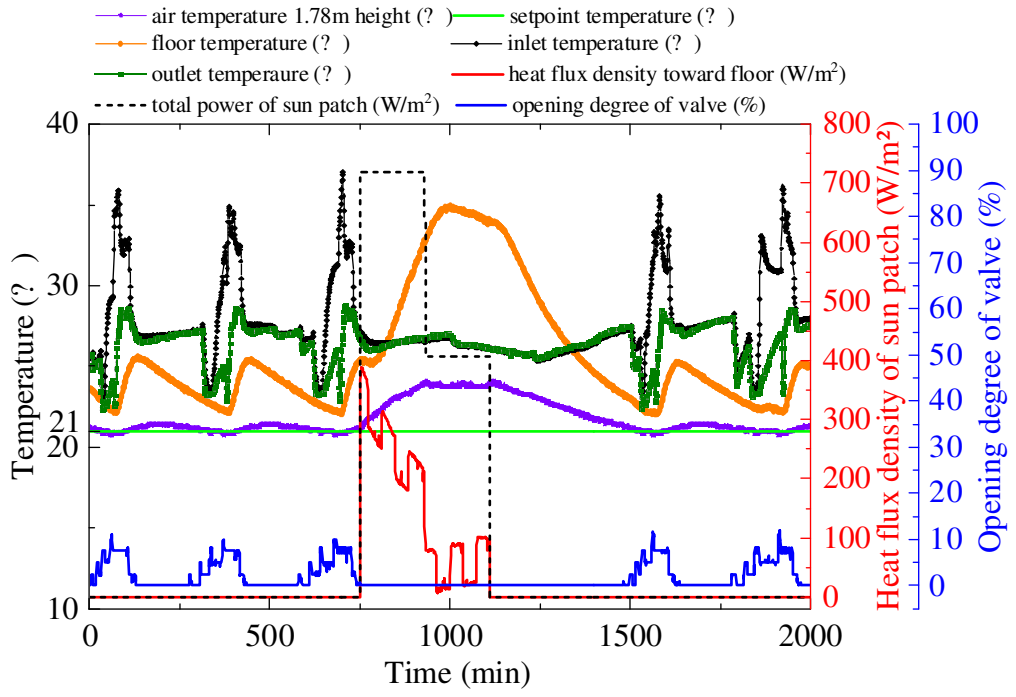

(b) profile 2

Fig. 12. The regulatory mechanisms of profile 1 and profile 2.

4. Thermal comfort evaluation

4.1. Overheating coefficients

In the second and third scenarios, since air temperatures were within the comfort zone, an overheating coefficient was proposed to describe the overheating efficiency of sun patch to a floor,

which was defined as the ratio of the overheating period of a floor to the sunshine duration marked by the arrows shown in Fig. 8(b). Fig. 13 shows the overheating coefficients of different sunshine durations. Thereinto, 6-1 and 6-2 represented profile 1 and profile 2 respectively. The overheating coefficients were up to 42.55% for 2 h, the highest 122.25% for 4 h, 112.69% for 6h, 94.8% for profile 1, and 107.05% for profile 2. Apart from the overheating phenomenon, Fig. 13 presented two important facts: the overheating coefficient was not positively associated with the sunshine duration, and the overheating coefficient also varied with the order of intensity change, even though the sunshine duration is kept same.

The facts that how the sun patch influenced the floor could be inferred. At the beginning, the thermal mass of floor contributed to preventing overheating, which consumed most of time and energy of 2h case. After that, the sun patch played a leading role in controlling the floor surface temperature, as a result, the overheating coefficient increased dramatically for 4h case. Referring to the Fig. 8 and Fig. 11 in the paper, the heat flux density of sun patch toward the floor was gradually decreasing when the floor surface temperature increased with time. That meant the growth rate of floor surface temperature decreased as well. Therefore the 6h case didn't get a higher overheating coefficient compared to the 4h case. Besides, the 6-2 case had a higher overheating coefficient than the 6-1 case, that was because the low-intensity solar radiation that first entered the room was used to preheat the floor, and it would also weaken the heating efficiency of the high-intensity solar radiation that entered the room later. But when the high-intensity solar radiation first entered the room, it would heat the floor and make the floor surface overheated faster, and the later low-intensity solar radiation would also extend the overheating period by slowing down the cooling process. Based on the experimental results, increasing the thermal mass of a floor and strengthening ventilation cooling could be considered to reduce overheating.

The overheating coefficient was not only related to the solar intensity and the sunshine duration, but also related to the order of intensity change. The case of 4h sunshine duration had a highest overheating coefficient among the cases with constant solar intensity of 718W/m^2. The overheating coefficient would be lower while the solar intensity varying from weak to strong in a day compared with the solar intensity varying from strong to weak in the condition of same sunshine duration. These findings could be a reference to the design of predictive control strategies considering the solar radiation.

Besides, the overheating coefficient could be used as an index of thermal comfort to evaluate thermal performance of buildings. These experiments were performed in the same building so the analysis mainly focused on variations of sun patch. But an overheating coefficient was also influenced by floor material and thickness, ventilation, and thermal insulation of envelope structure.

It could be adopted by building designers to compare thermal performance of different buildings in preventing overheating by solar radiation for design or control purposes.

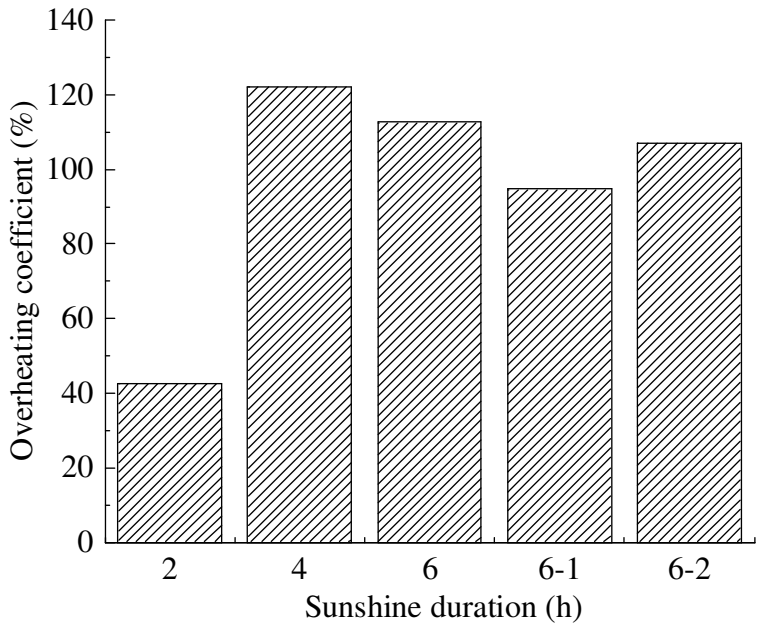

Fig. 13. The overheating coefficient of sun patch for different sunshine durations.

4.2. Vertical air temperature difference

Aside from the overheated floor, a high vertical air temperature difference between head and ankles can also cause the local thermal discomfort. ASHRAE 55-2017 standard [29] gives the condition that provides thermal comfort for air temperature difference between head level and ankle level, which shall not exceed 3℃ for seated occupants. Table 3 illustrates the vertical air temperature difference at 1.1 and 0.1 m (head level and ankle level temperatures for a seated person) on which ISO7730:2005(E) [30] is based for the classification of occupied spaces with respect to thermal comfort requirements.

Table 3
Categories for the local thermal discomfort [30].

Category	Vertical air temperature difference (℃)
A	<2
B	<3
C	<4

For the benchmark scenario, the temperature difference lower than 2℃ was under limitations for buildings classified in Category A, as shown in Fig. 14(a). The horizontal straight lines in green

represented the upper limit of A category in Fig. 14. As it could be seen, the temperature difference variation was of periodic fluctuation following the opening rate of the valve. Due to being closer to the floor, the air temperature at 0.1m height increased rapidly faster than the one at 1.1m height when the valve started, and the corresponding temperature difference would decrease at this time. Then, the valve closed, and the air temperature at 0.1m height decreased rapidly faster than the one at 1.1m height, so the temperature difference would rise up. Consequently, the peak change of the air temperatures and the temperature difference was completely opposite. For the scenarios with sun patch, all of them changed from category A to category B, and the temperature difference was less than 3℃ and partly more than 2℃. During the sunshine duration, the air temperature at 1.1m height increased rapidly faster than the one at 0.1m height shown in Fig. 14(b-f), therefore, the temperature difference rose gradually. This was due to the fact that the air temperature only depended on the sun patch when the valve was maintained closed at this stage, and influenced by the natural convection, the hot air from the heating film located at one side of the air temperature sensors shown in Fig. 5, rose up first and then went down from the sides.

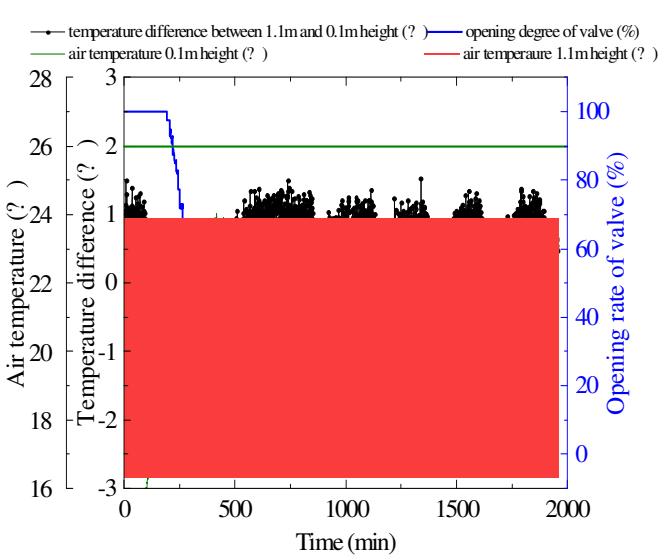

(a) the primary stage

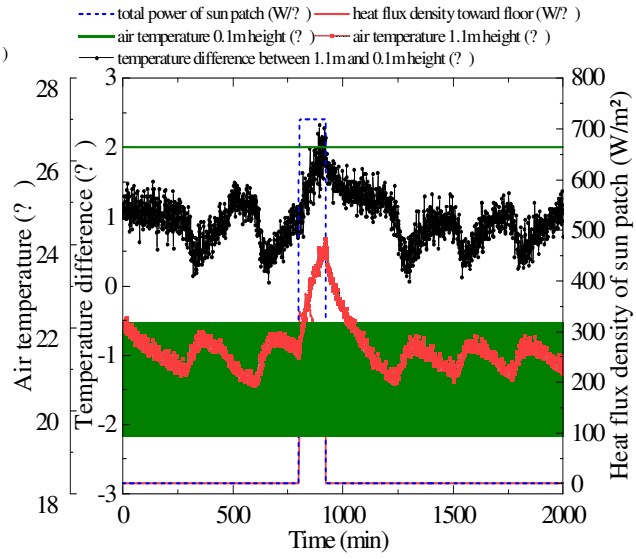

(b) 2h of sunshine duration

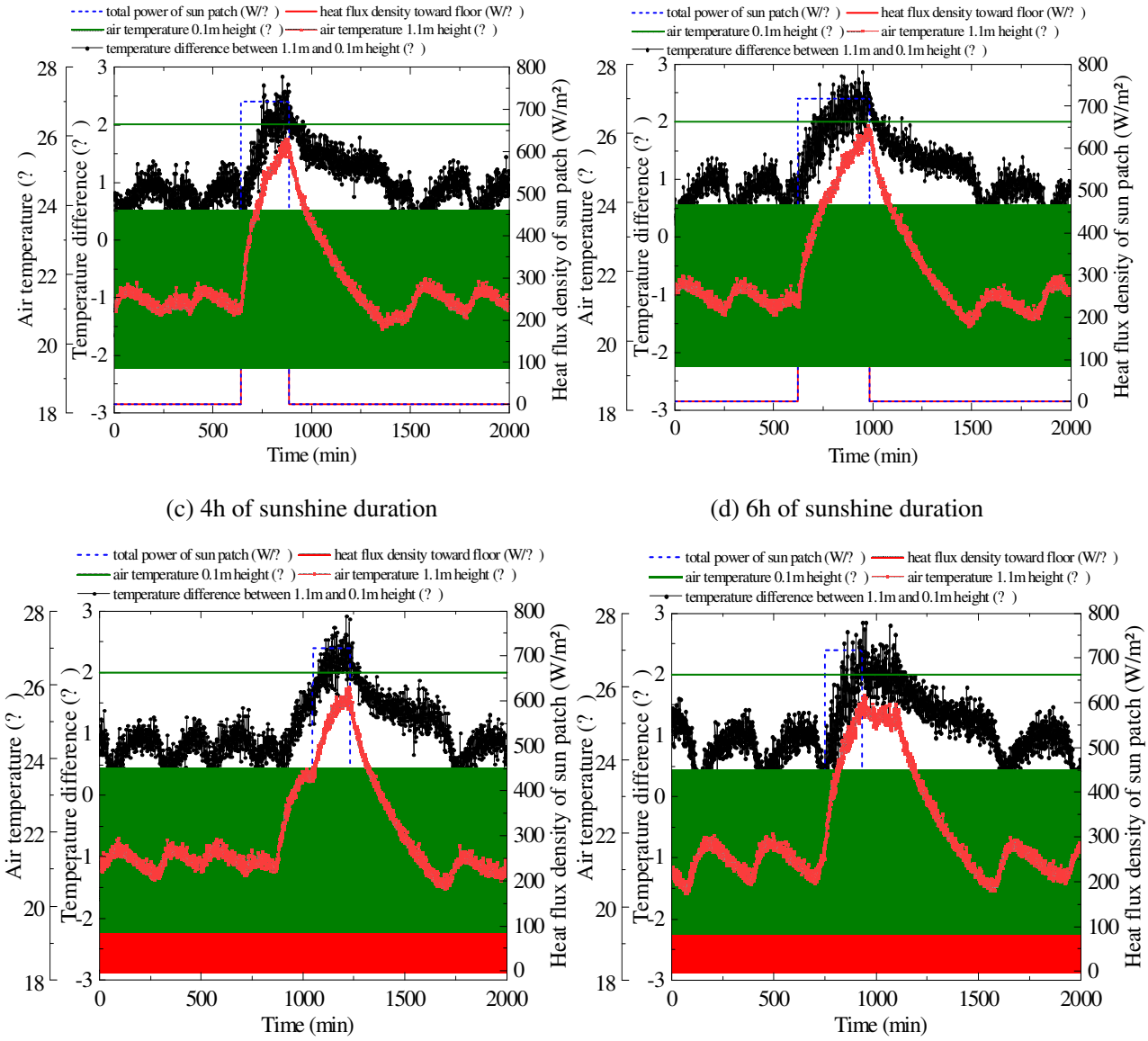

(c) 4h of sunshine duration

(d) 6h of sunshine duration

(e) profile 1

(f) profile 2

Fig. 14. Air temperature difference variation between 1.1m and 0.1m height for all scenarios.

In general, the vertical air temperature difference for all cases was within the comfort zone according to ASHRAE 55-2017 standard [29], whereas ISO7730:2005(E) [30] classified them as category A and category B in terms of different thermal comfort requirements. When the sun patch was applied on the floor, the vertical air temperature difference increased as well as the indoor air temperature as depicted in Fig. 14, and the building type changed from category A to category B. To quantify the impacts of sun patch, the share of B category duration against the sunshine duration was shown in Fig.15. It was found that the ratios were 27.6%, 72.1%, 90.2%, 53.2% and 84.8% for 2, 4, 6 hours and 6-1, 6-2, respectively, among which the maximum was in the case of 6h. Fig. 15 also presented two important facts: the share of B category duration increased with the sunshine duration, and the different order of intensity change in the condition of same sunshine duration would lead to different B category duration. Namely, the B category duration would be much longer

while the solar intensity varying from strong to weak in a day compared with the solar intensity varying from weak to strong.

The facts that how the sun patch influenced the air could be inferred. Referring to the Fig. 8 and Fig. 11, the heat flux density of sun patch toward the floor was decreasing gradually with the floor surface temperature increasing, which meant the heat flux density of sun patch toward the air was increasing gradually by natural convection. Therefore the effect on air temperatures would be stronger with the sunshine duration. The air temperature at 1.1m height increased rapidly faster than the one at 0.1m height, which influenced by natural convection. As a result, the share of B category duration increased with the sunshine duration. For the case of 6-1, the vertical air temperature difference during the first three hours with low-intensity solar radiation didn't exceed the limit of A category as shown in Fig. 14, while the first with high-intensity solar radiation made it exceeding the limit of A category in the case of 6-2 and the later three hours remained it there. Hence, the case of 6-2 was much worse than the case of 6-1.

When a category A building is designed for very sensitive or fragile persons, the direct solar radiation must be taken into account. This study also provides an experimental base for category A building designers.

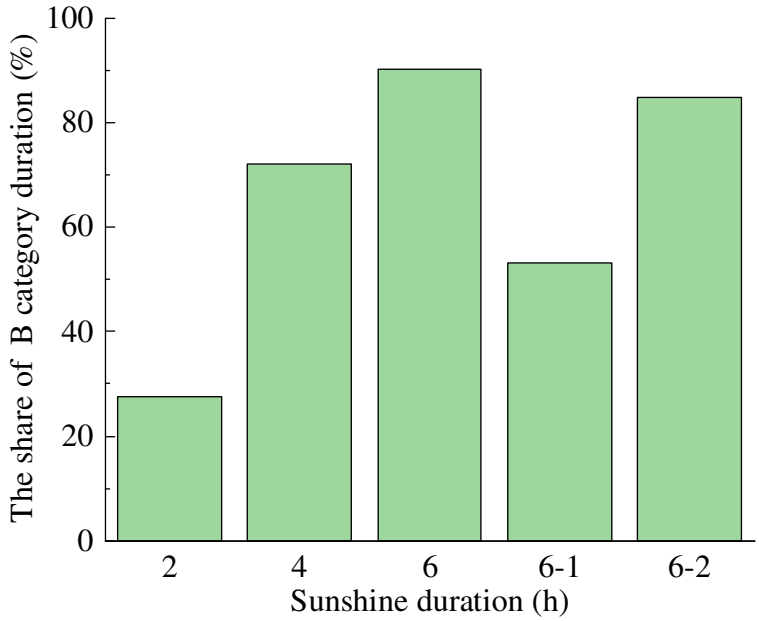

Fig. 15. The share of B category duration against the sunshine duration.

5. Conclusion

In this experimental work, the impact of the sun patch on the indoor thermal comfort was studied via a heating film, which was adjusted to realize different scenarios in terms of the sunshine duration and solar intensity according to the local climate data. Conclusions are as follows:

1. The sun patch led to the floor overheating problems under the existing control system. The maximum floor surface temperatures were 29.5℃, 35.7℃ and 37.3℃ for 2, 4 and 6 hours of sunshine durations, and 36.4℃, 34.97℃ for profile 1 and profile 2, exceeding the limitation of 29℃. An overheating coefficient was proposed to describe the overheating efficiency of sun patch to a floor. The overheating coefficients were 42.55% of 2 hours, 122.25% of 4 hours, 112.69% of 6 hours, 94.8% for profile 1, and 107.05% for profile 2. The overheating coefficient was not only related to the solar intensity and the sunshine duration, but also related to the order of intensity change. The case of 4h sunshine duration had a highest overheating coefficient among the cases with constant solar intensity of 718W/m^2. The low-intensity solar radiation that first entered the room preheated the floor, which would weaken the heating efficiency of the high-intensity solar radiation that entered the room later. Therefore the overheating coefficient would be lower while the solar intensity varying from weak to strong in a day compared with the solar intensity varying from strong to weak in the condition of same sunshine duration. These findings could be a reference to the design of predictive control strategies considering the solar radiation. Besides, the overheating coefficient could be used as an index of thermal comfort to help building designers to compare thermal performance of different buildings in preventing overheating by solar radiation for design or control purposes.

2. The vertical air temperature difference for all cases was within the comfort zone according to ASHRAE 55-2017 standard, whereas ISO7730:2005(E) classified them as category A and category B in terms of different thermal comfort requirements. For the benchmark scenario, the vertical air temperature difference was under limitations of category A buildings. When the sun patch was applied on the floor, the building type changed from category A to category B. The shares of B category duration against the sunshine duration were 27.6%, 72.1%, 90.2%, 53.2% and 84.8% for 2, 4, 6 hours and profile 1, profile 2, respectively. The heat flux density of sun patch toward the floor was decreasing gradually with the floor surface temperature increasing, which meant the heat flux density of sun patch toward the air was increasing gradually by natural convection. Therefore the effect on air temperatures would be stronger with the sunshine duration. This study shows the adverse effect of sun patch on category A buildings and also provides an experimental base for category A building designers.

3. To sum up, the thermal discomfort was not only related to the solar intensity and the sunshine duration, but also related to the order of intensity change, and the case of 6h sunshine duration would lead to the worst living conditions taking all these factors consideration.

4. The floor heating system regulated the air temperature according to the setpoint by controlling the opening rate of thermostatic valve, which could meet the general heating requirement without sun patch, but couldn’t avoid the overheating problems induced by sun patch

by only closing the valve fully. Based on it, there are some control strategies' improvements in the future. For example, reducing the setpoint value within comfort range or giving a setpoint curve versus the climate data if possible, or monitoring the floor surface temperature with the constant setpoint. As an available solution, the outlet water probably can be used as the inlet water to cool down the floor while the sun patch is coming and the floor surface temperature is beyond acceptable tolerances. Besides, increasing the thermal mass of a floor and strengthening ventilation cooling could be considered to reduce overheating. A solar shading could be used in category A buildings if necessary.

The future contribution could be to work on the optimal control of PID considering the impact of sun patch to improve the overall system performance. Besides, it's also necessary to make efforts to study on the variation of position, shape and intensity of real sun patch projected onto the floor surface of the residence so as to adjust the heating film to match the real situation well.

Acknowledgments

The authors gratefully acknowledge financial support from China Scholarship Council (No.201908120112), Grand-Est Region, Troyes Champagne Métropole, European Regional Development Fund, and EPF Foundation.

References

[1] Statistical Office of the European Union (Eurostat). Available at: http://ec.europa.eu/eurostat/web/energy/data/main-tables. [Accessed 1 September 2020].

[2] Xu X., Wang S., Wang J., Xiao F., Active pipe-embedded structures in buildings for utilizing low-grade energy sources: A review. Energy and Buildings 2010;42(10):1567-1581.

[3] Olesen B. W., Radiant Floor Heating in Theory and Practice. ASHRAE Journal 2002; (7):19-26.

[4] Hu M., Xiao F., Jørgensen J. B., Li R., Price-responsive model predictive control of floor heating systems for demand response using building thermal mass. Applied Thermal Engineering 2019;153:316-329.

[5] Rhee K. N., Olesen B. W., Kim K. W., Ten questions about radiant heating and cooling systems. Building and Environment 2017;112:367-381.

[6] Merabtine A., Kheiri A., Mokraoui S., Belmerabet A., Semi-analytical model for thermal response of anhydrite radiant slab. Building and Environment 2019;153:253-266.

[7] Zheng X., Han Y., Zhang H., Zheng W., Kong D., Numerical study on impact of non-heating surface temperature on the heat output of radiant floor heating system. Energy and Buildings 2017;155:198-206.

[8] Cho J., Park B., Lim T., Experimental and numerical study on the application of low-temperature radiant floor heating system with capillary tube: Thermal performance analysis. Applied Thermal Engineering 2019;163:114360.

[9] Lu S., Tong H., Pang B., Study on the coupling heating system of floor radiation and sunspace based on energy storage technology. Energy and Buildings 2018;159:441-453.

[10] Yun B. Y., Yang S., Cho H. M., Chang S. J., Kim S., Design and analysis of phase change material based floor heating system for thermal energy storage. Environmental Research 2019;173:480-488.

[11] Zhang L., Huang X., Liang L., Liu J., Experimental study on heating characteristics and control strategies of ground source heat pump and radiant floor heating system in an office building. Procedia Engineering 2017;205:4060-4066.

[12] Zhao J., Lyu L., Han X., Operation regulation analysis of solar heating system with seasonal water pool heat storage. Sustainable Cities and Society 2019;47:101455.

[13] Zhao J., Lyu L., Li X., Numerical analysis of the operation regulation in a solar heating system with seasonal water pool thermal storage. Renewable Energy 2019.

[14] Brideau S. A., Beausoleil-Morrison I., Kummert M., Effects of controls and floor construction of radiant floor heating systems for residential application with high variability of solar gains. Science and Technology for the Built Environment 2020;0:1-17.

[15] MacCluer C., The response of radiant heating systems controlled by outdoor reset with feedback. ASHRAE Transactions 1991;97(2):795–9.

[16] Hassan M. A., Abdelaziz O., Best practices and recent advances in hydronic radiant cooling systems - Part II: Simulation, control, and integration. Energy&Buildings 2020;224:110263.

[17] Gwerder M., Tödtli J., Lehmann B., Dorer V., Güntensperger W., Renggli F., Control of thermally activated building systems (TABS) in intermittent operation with pulse width modulation. Appl. Energy 2009;86:1606–1616.

[18] Romani J., Gracia A., Cabeza L. F., Simulation and control of thermally activated building systems (TABS). Energy and Buildings 2016;127:22-42.

[19] Guo H., Aviv D., Loyola M., Teitelbaum E., Houchois N., Meggers F., On the understanding of the mean radiant temperature within both theindoor and outdoor environment, a critical review. Renewable and Sustainable Energy Reviews 2020;117:109207.

[20] Athienitis A. K., Investigation of thermal performance of a passive solar building with floor radiant heating. Solar Energy 1997;61(5):337-345.

[21] Candanedo J. A., Allard A., Athienitis A. K., Predictive control of radiant floor heating and transmitted irradiance in a room with high solar gains. ASHRAE Transactions 2011.

[22] Olesen B. W., Comparative experimental study of performance of radiant floor-heating systems and a wall panel heating system under dynamic conditions. ASHRAE Transactions 1994;100 (1):1011–23.

[23] Beji C., Merabtine A., Mokraoui S., Kheiri A., Kauffmann J., Bouaziz N., Experimental study on the effects of direct sun radiation on the dynamic thermal behavior of a floor-heating system. Solar energy 2020;204:1-12.

[24] Benzaama M. H., Lachi M., Maalouf C., Mokhtari A.M., Polidori G., Makhlouf M., Study of the effect of sun patch on the transient thermal behaviour of a heating floor in Algeria. Energy and Buildings 2016;133:257-270.

[25] Rodler A., Virgone J., Roux J. J., Hubert J. L., Development and validation of a three dimensional thermal transient numerical model with sun patch: Application to a low energy cell. Energy and Buildings 2015;87:425-435.

[26] Rodler A., Virgone J., Roux J. J., Adapted time step to the weather fluctuation on a three dimensional thermal transient numerical model with sun patch: Application to a low energy cell. Energy and Buildings 2017;155:238-248.

[27] Almeida Rocha de A. P., Rodler A., Oliveira R. C.L.F., Virgone J., Mendes N., A pixel counting technique for sun patch assessment within building enclosures. Solar Energy 2019;184:173-186.

[28] 2016 ASHRAE Handbook. Heating, Ventilating and Air-Conditioning Systems and Equipment: air-conditioning and heating systems.

[29] ANSI/ASHRAE Standard 55-2017. Thermal Environmental Conditions for Human Occupancy.

[30] ISO 7730:2005(E). Ergonomics of the thermal environment-Analytical determination and interpretation of thermal comfort using calculation of the PMV and PPD indices and local thermal comfort criteria.

[31] Monthly Climate in Troyes. Available at: https://www.infoclimat.fr/climatologie-mensuelle/07168/janvier/2020/troyes-barberey.html. [Accessed 20 January 2020].